UNIVERSITY OF TWENTE.

Faculty of Science and Technology

A Methodology on Analyzing Pressurized Lip Seal Geometry under Misalignment through Glass

Thomas Giorgio

B.Sc. Thesis
August 2019

Supervisors:
Dr.Ir. M.B.de Rooij

Advanced Technology
Faculty of TNW,
University of Twente
P.O. Box 217
7500 AE Enschede
The Netherlands

Contents

Chapter 1

Introduction

Sealing has been used in many engineering applications. *Aegir-Marine BV* uses sealing on stern-tube. The stern-tube shaft is a part that connects propeller and an engine on a ship where this two parts are separated by a sealing component namely stern-tube seal. It prevents oil leakage from the engine part to the sea and vice versa. The stern-tube seal is built up from radial-shaped elastic material (lip seal) and clamped between two metal disk which are known as the housing. As the ship size increases, the stern-tube depth increases with respect to the sea level resulting on unbalance pressure between the water side and the oil side. Therefore, this research will deal with pressurized seal.

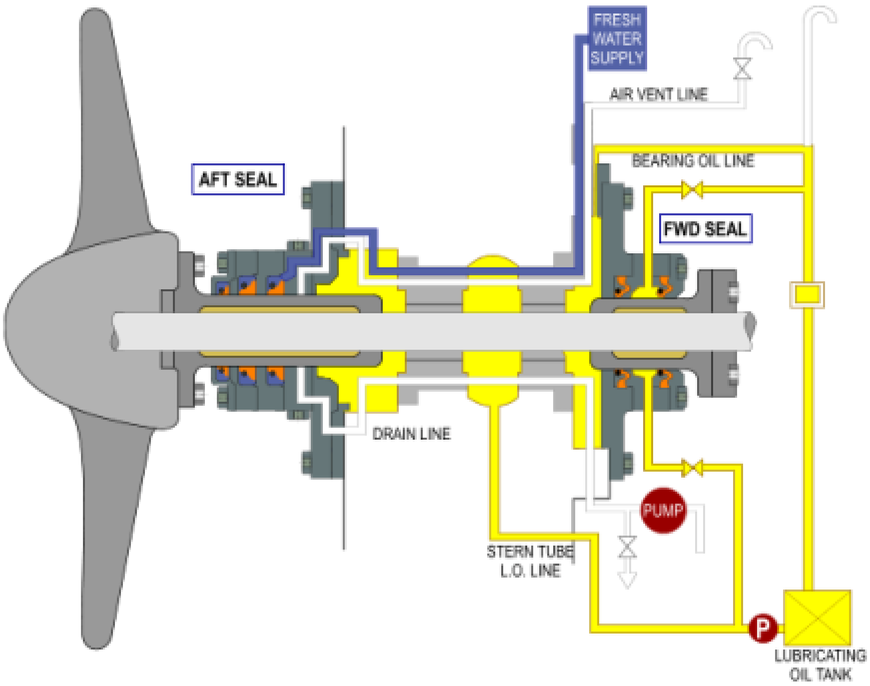

Figure 1.1: Stern tube seal configuration (Source: Marine Insight)

1.1 Leakage

The purpose of sealing is to prevent oil leakage, however, oil leakage still occurs in practice. Oil leakage occurred more often during static condition. [1]. When the contact pressure between the shaft and the lip seal is not high enough, microscopic leakage paths will start to appear in the contact width area and hence allowing the oil to pass through and causes leakage. The oil leakage is also dependent on the seal performance. The seal performance is influenced by the loading and the geometry of the seal [2]. To understand more about the seal performance, variables and parameters are needed to be explained before addressing the problems. The variables and parameters will be explained on the following subsections.

1.1.1 Lip seal Geometry

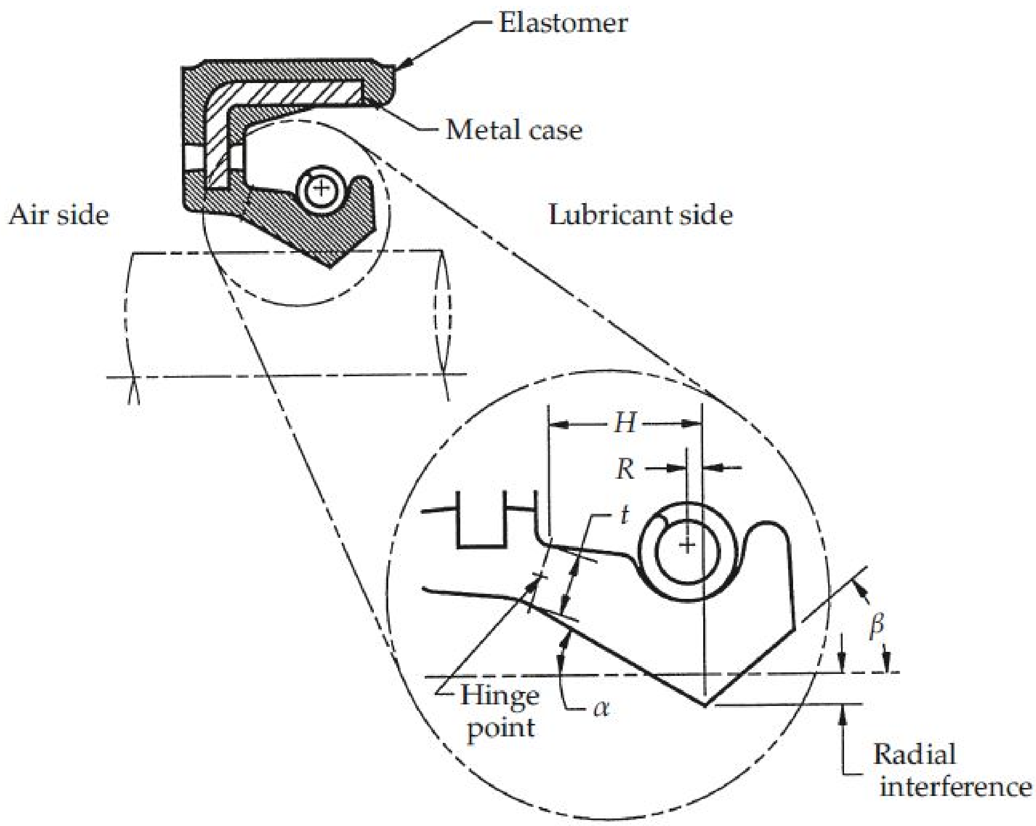

Figure 1.2: Lip seal Geometry (Source: Wennehorst, 2016)

Before discussing the problems of this research, in more detail, the geometry on a lip seal must first to be defined (see picture 1.2). The lip seal works by using reverse pumping action mechanism which provides dynamic tightness under lubricated conditions. By unbalancing the contact pressure distribution the maximum lies closer to the oil side, thus, the reverse pumping mechanism can be obtained. Due to this condition the pressure distribution is axial-asymmetric. By differentiating the angles size where the angle α (see figure 1.2 must be less than β, where the region α is also known as the air side and the β region is the lubricant or oil side. Second, the axial distance R between the seal lip contact band and the center-line of the spring [3]. It is necessary to define the lip-seal geometry in order to understand more about the deformation of the lip seal contact width and the lip seal deformation where these parameters commonly used to validate simulation model.

1.1.2 Static Eccentricity

Static eccentricity is a condition where a non-uniform clearances occurs in circumferential direction at both the oil and the air side of the seal. These clearances contributes to a non-uniform contact pressure distribution and contact width in the circumferential direction. Moreover, the axial position of the lip will vary in the circumferential direction and the boundaries of the contact zone become slanted [4]. The misalignment under static eccentricity can be categorized into two types which will be explained further on the following paragraph.

Misalignment

The static eccentricity can be categorized into two types, which are; *Bore eccentric misalignment* and *angular misalignment*. Bore eccentric misalignment is a condition where the lip seal center is oftentimes not perfectly aligned with the center of the rotary shaft. This misalignment causes the lip to be pressed on one side and the contact force on another side is reduced, hence, the contact area between the lip seal and the rotary shaft is reduced. While angular misalignment is a state where one side of the lip seal is skewed on the axial direction causing the seal to stretch in a slanting oval shape around the shaft [5].

1.1.3 Pressure Difference

The stern tube seal operates normally by generating slightly higher pressure difference on the oil side than the air side which leads to a slight positive pressure difference . Under certain circumstances, the pressure difference between the oil side and the air side is greater than the normal operating pressure difference, therefore, The lip seal geometry (see subsection 1.1.1) will be deformed by the pressure difference. Assuming that no bore-eccentricity misalignment is applied, as positive pressure difference applied (positive pressure difference is defined when the absolute pressure on the oil side is bigger than the air side) , the lip-seal contact area width increases and the thickness is radially equal along the shaft axis. On the other hand, the contact area width decreases as negative pressure difference is applied [5] [6]. The contact area width is not equal along the shaft axis when the bore-eccentric misalignment is introduced.

1.2 Previous research

As has been stated in subsection 1.1.3 and subsection 1.1.2, the contact area width will increased as the pressure difference increased and the deformed contact lip seal will be nonuniform on the circumferential direction. Therefore, It is necessary to capture this non uniformity deformed lip seal. FEM simulation has been done to predict the lip seal deformation, moreover, the actual measurement of the lip seal deformation has been used to validate the FEM model. Several researches have been done to obtain the lip seal deformation. The lip seal deformation is calculated by using quartz shaft and laser system. however this research focused on dynamic state of rotating shaft seals [7]. Using a similar setup, the static state contact area width measurement has been done by Twente university [6]. The lip seal deformation is measured by using the misaligned distance which calculated by using total internal reflection (TIR) method. By using the difference in refractive indices between the glass and air, the laser bounces back inside the shaft until the laser hit the seal-shaft interface, reflecting the laser. The reflected laser shows illumination of the contact interface and captured by using a camera *Dinocapture 2.0*. The lip seal deformation is calculated on prescribed points around the shaft diameter and the result was interpolated between each measurement points. However the method of this measurement requires initial calibration for each picture that is taken. The calibration is required due to the eccentric misalignment between the center of the rotating disk and the center of the shaft. Another measurement that has been done by Stuttgart university is to inject epoxy in between the shaft. Letting the epoxy to solidify and removing the solidified epoxy, the lip seal deformation can be measured. However, by using this method, a new lip seal must be replace regularly for each measurement.

1.3 Problem Formulation

To sum up, The deformation of a pressurized lip seal under missalignments is the focus of this research, in addition, The seal-shaft contact problem is a nonlinear problem due to the non-linearity of the geometrical, physical and boundary conditions. Consequently, the analytic solution is too complex to be derived, however, the contact problem still can be predicted and analyzed by using finite element method (FEM) [8]. Therefore, This research focuses on introducing a method to measure the contact area width boundary location and the deformed contact area width along the shaft circumference. To see how the contact area width and the contact area boundaries deformed, as an illustration, see figure 3.12. However, the discussion over the deformation will be discussed in the corresponding chapter. Furthermore, comparing and discussing the results with the existing research. the boundary condition of this research is that all measurements will be treated in static condition. Therefore the time dependent variables on the lip seal deformation is neglected. In addition, temperature effects on the lip seal will be put aside. There are two independent variables that in this research will be tested on which are; the pressure differences between the air side and the oil side, and bore-eccentricity misalignment. To summarize, the problems can be formulated into two questions which are;

1. How to measure the lip seal deformation?

2. How does the pressure difference and the bore eccentricity misalignment affect the contact area width and the contact width boundary position?

Chapter 2

Methodology

The lip seal deformation is measured by using digital image processing tools from *matlab* on the camera images obtained. By Using the total internal reflection method (TIR) the contact area width can be visualized and the contact area width illumination is reflected to a 45 degrees skewed mirror and the image reflection is captured by a camera. The goal of this measurement is to measure the contact area width with respect to the location of the shaft and the lip seal deformation profile. The process of the measurement will be explained thoroughly in the following sections.

2.1 test rig

Before discussing further on the measurement of the lip seal deformation, understanding the test rig is important. To measure the contact area width, a rubber lip seal is clamped between a glass shaft of 200mm diameter with aluminum frame (The red-colored part (see figure 2.1). the lip seal is seated on the bottom housing slot. The bottom housing slot is then screwed to a top housing slot. The misalignment can be achieved by sliding the bottom slot with respect to the bottom cover with allowed maximum misalignment of 1.5mm. The radial position 'zero' is the reference point where the misalignment always applied on. In order to achieve the wanted misalignment, the reference point on the bottom slot is then pushed maximally towards the glass shaft and then from the opposing side is pushed slowly until the wanted misalignment is achieved.

2.1.1 Turning table, mirror, and camera placement

A turning table is placed in the center of the hollow cavity of the shaft where a fourty-five degrees skewed mirror is mounted on the turning table. The turning table is a two separated component which are the stator and the motor. The motor rotates

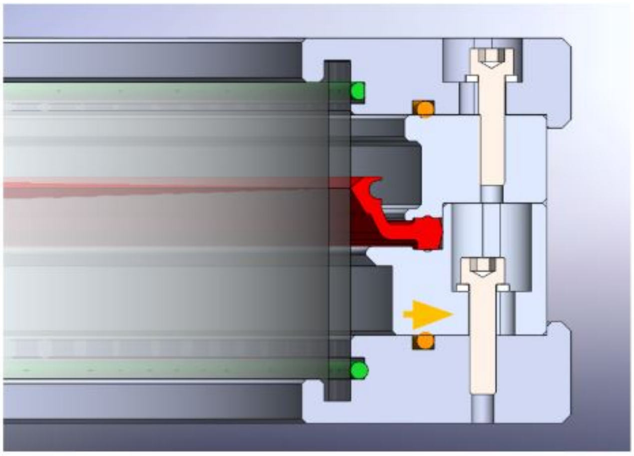

Figure 2.1: Test rig sectional view

around the hollow part of the stator where stator makes sure that the eccentricity between the center of the shaft and the center of the motor are aligned. A camera is then placed on top of the mirror hence, the camera rotates simultaneously with the mirror taking images from 24 different points along the circumference. The distance between the camera and the mirror can be varied for as long the camera can capture a clear image. The reason of the placement between the camera and the mirror will be explained in the following section (see figures 2.2 and 2.3).

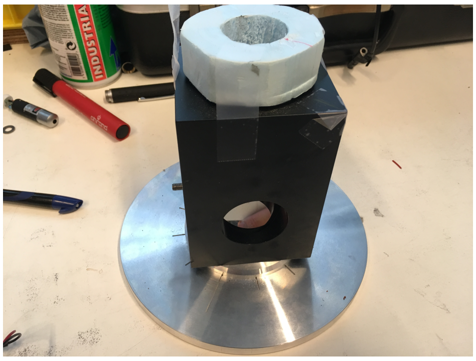

Figure 2.2: Mounted mirror on top of the rotating disk

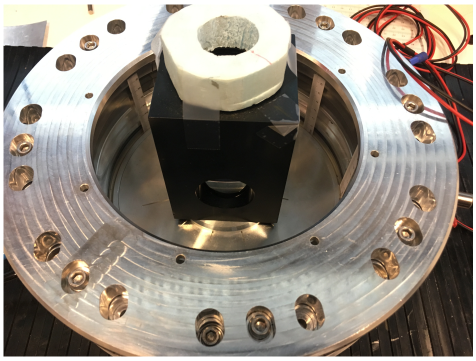

Figure 2.3: Installed rotating disk inside the test rig

2.2 Image Processing

Boundary detection method is used to analyzed the lip seal deformation. As what has been stated on the problem formulation (see 1.3) the contact area width is measured from two different approaches. The first approach is by edge detection technique and secondly, Hough transform approach is used to acquire the lip seal boundary location where from this acquired location, the contact area width can be calculated. Both approaches is required to be done where the reason of this will be discussed on the following chapter. To sum up, the image processing process is described on figure 2.4.

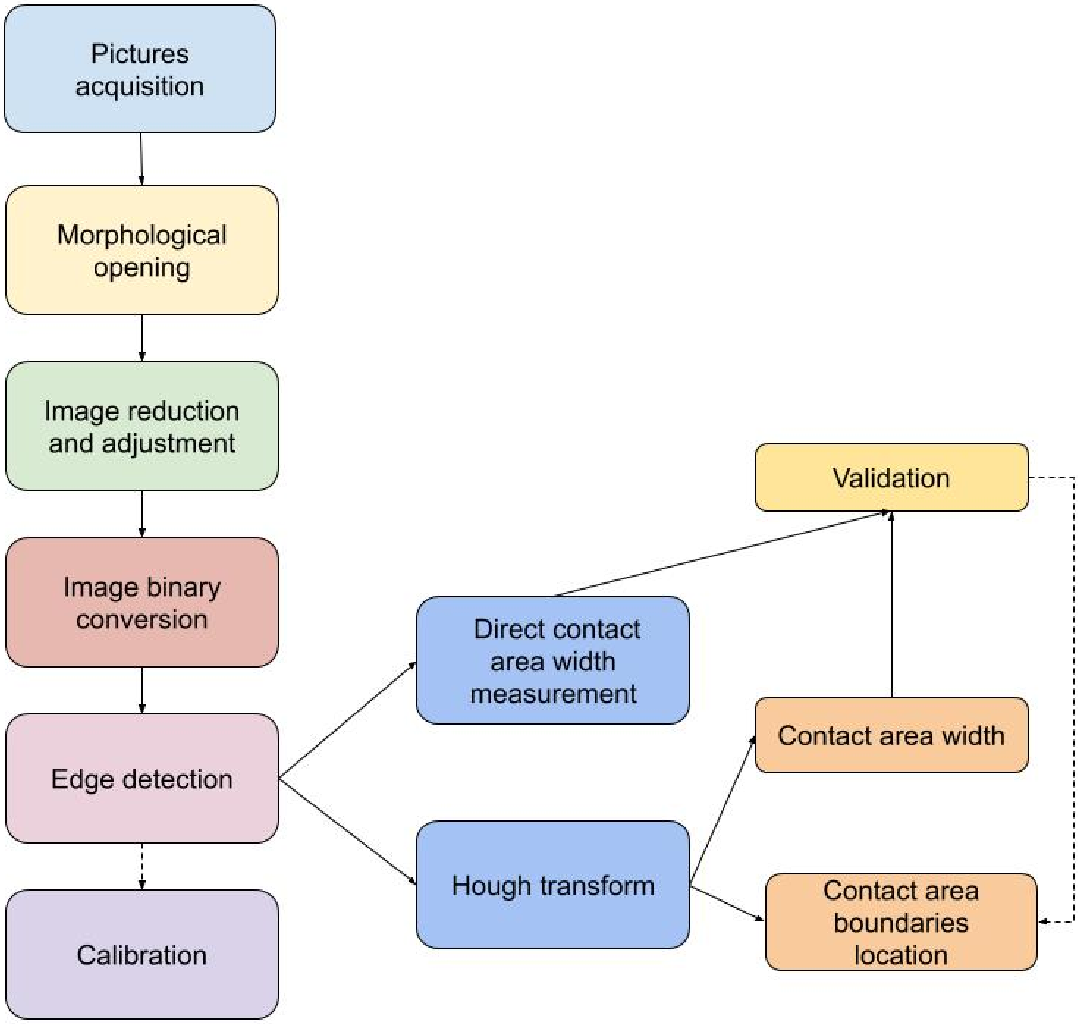

Figure 2.4: Flowchart of image processing

2.2.1 Boundary Detection Method

The first step to measure the contact area width is to calibrate the measurement. The purpose of this calibration is to scale the actual length of the image with the number of pixels. In order to calibrate the raw image is cropped resulting top left image (see figure 2.5). The purpose of cropping image is to remove any other object in the picture that will affect the image processing process.

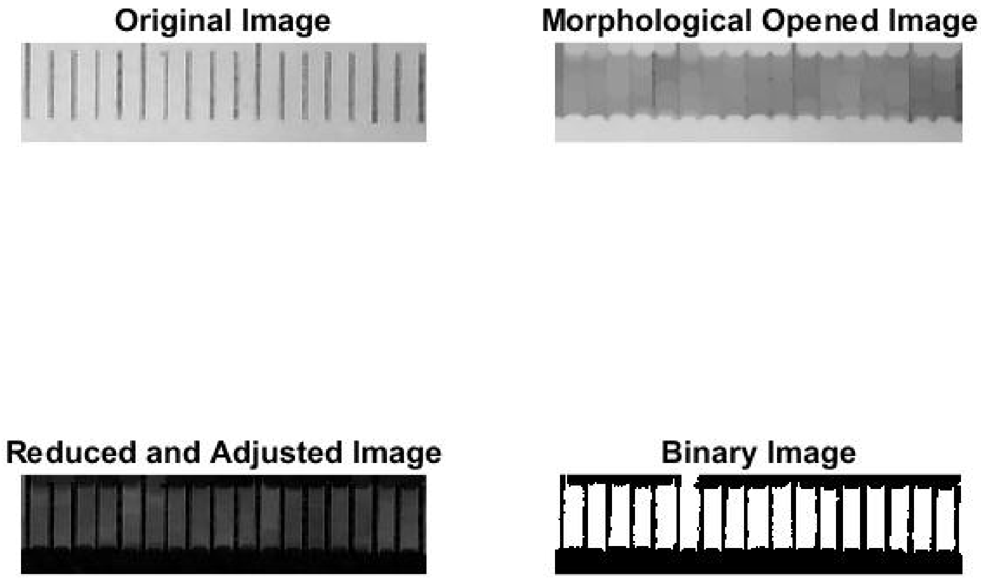

Figure 2.5: Image processing (Start from top left, top right, bottom left, and finally bottom right)

It is also important to note that the size of the image does not change when the image is cropped.

Morphological Opening

Morphological opening is a method to construct an image with an element structure with certain size of pixel. As can be seen on the original image, the background of the image is uneven. Therefore, morphological opening is necessary to uniform the background of the image. Looking at top right figure 2.5, the selected part is the bright colored region, however several part in the region of the measurement line has darker image. Hence, by reducing the original image from the morphological opened image, the region between each measurement lines will remain bright where the distance between two lines is one millimeter.

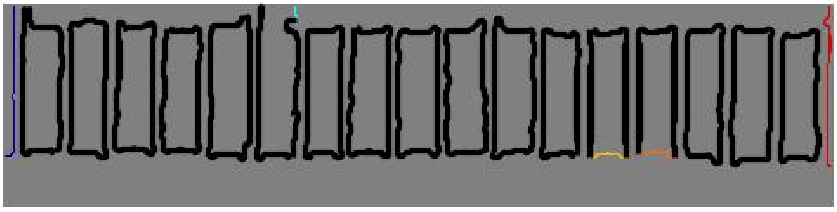

Figure 2.6: detected edge

Edge Line detection

Before the edges of the image can be detected, the reduced and adjusted image has to be converted into binary image. Using a built in *Matlab* function *threshold*, the brighter part region is conserved. The *threshold* function will average the gray-scale intensity level from whole picture, hence, the brighter colored region will set as ”1” (which is white) and ”0” (which is black) where this process resulted the binary image version. After the image converted into binary image, the edge detection function can be applied (see figure 2.6). Each boundary positions is stored into groups of vectors where each vector represents the boundary coordinates of each rectangular-shaped detected boundaries.

Contact Area Width

The method of image processing for contact area width is the same as the calibration process. Color filtration can be used to have better image acquisition (Depends on which laser color is used). The contact area width is measured by measuring the absolute distance between two points that located on the same y-coordinate whereas on the calibration process to determined the pixel distance within 1mm. Knowing the separation distances in pixels, the distance is then converted into millimeter unit. By using this technique, the distance between the camera and the mirror is not necessary to be defined for as long the image taken is focused.

Lip Seal Deformation Profile

The lip seal boundary location can be measured by measuring the absolute distance between the bottom housing and the contact area boundary position. On figure 2.8, the object that bounded by orange-colored boundaries is the bottom housing, while the the green-shaded region that surrounded by blue-colored boundaries is the lip

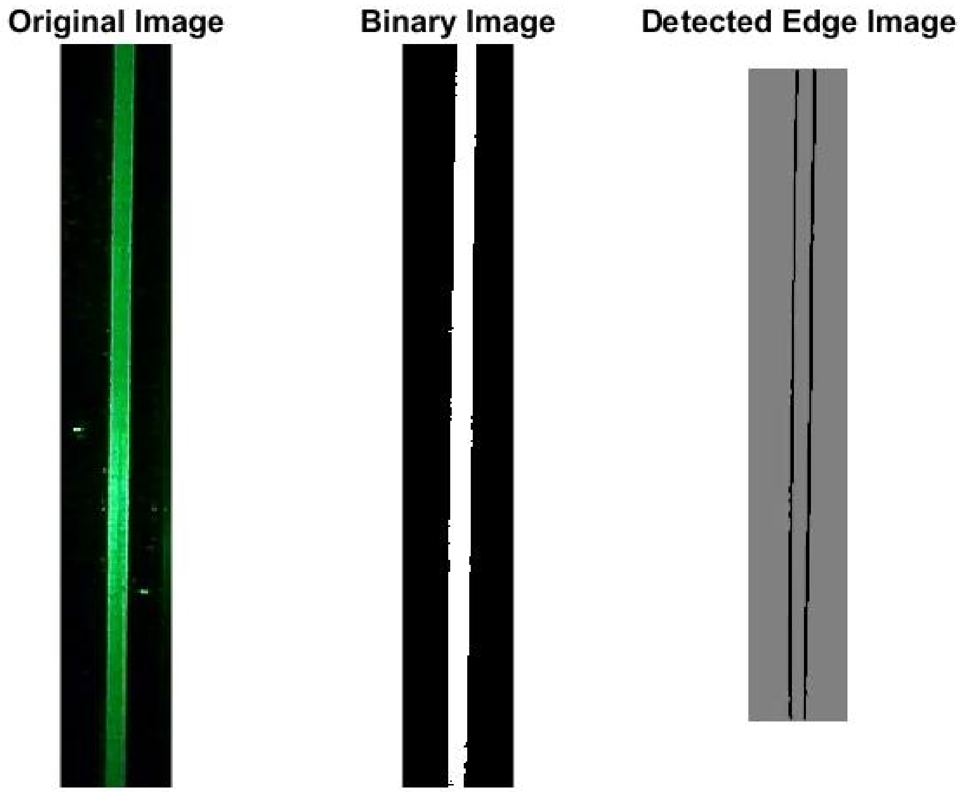

Figure 2.7: Contact area width image processing process

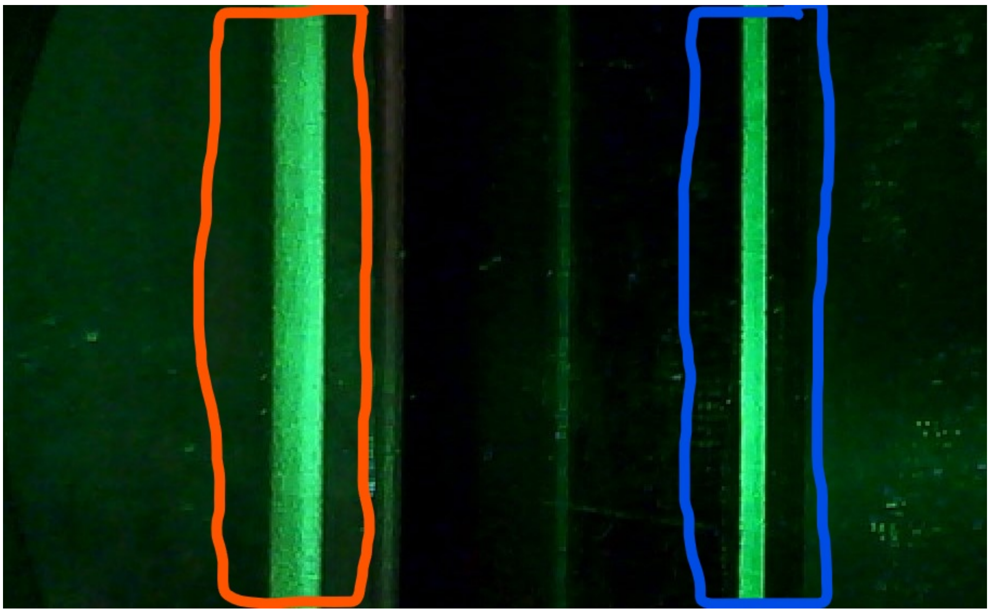

Figure 2.8: Original Image

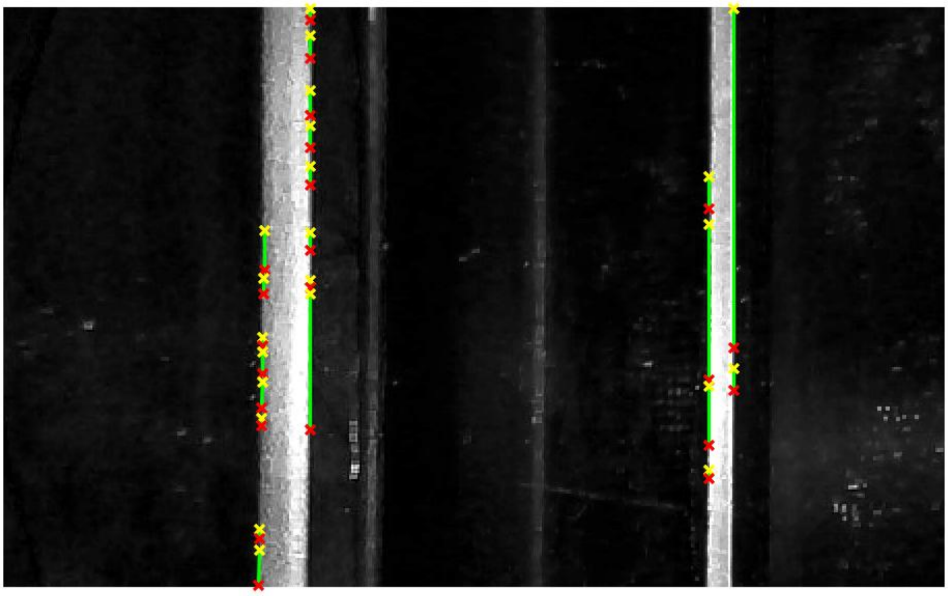

Figure 2.9: Detected lines by using hough transform

seal contact area. The absolute distance is then taken from the right side edge of the bottom sealing to the edge of the contact area width boundaries.

The distance can be measured by Hough transform. The function of Hough transform is to detect lines that exist in a specimen. Before transforming the image with Hough transform, the image must be converted to binary image. Using the boundary detection method, the edge of the housing and the illuminating deformed lip seal can be identified. As can be seen on figure 2.10, the distance between x-coordinates between the housing and the lip seal contact area boundaries can be measured which resulted two different distances which are; the inner and outer boundaries positions. Finally by interpolating all the boundary locations, the lip seal deformation profile can be achieved.

Hough Transform

As what has been stated before, the Hough transform detect lines from the processed image. To understand how Hough transform works, first, imagine that a line lying on a two dimensional XY-plane. The line can be describe in a mathematical sentence as stated on equation 2.1. This XY-plane represents the real image. The line on this plane is then divided into finite amount of coordinates. To analyze whether there is a line on the image, the coordinates is then converted into paramemter plane where m, the gradient, is the x-axis and b is the y-axis, conversely, the x coordinate on the XY-plane becomes the gradient on the parameter plane and y coordinate becomes the constant. On the parameter plane, using the x and y coordinates from the XY-plane, multiple values of m and b are run to construct lines based on a single coordinate. This process is repeated to every coordinates that lie on the XY-plane to the parameter plane. As the lines on the parameter plane intersect, the highest coordinate frequency where the lines are intersected, the coordinate is taken and fitted back to the real image plane, resulting in one solid line. However, matlab uses polar coordinates on the parameter plane where the line equation in polar coordinate is stated on equation 2.2

$$y = mx + b \tag{2.1}$$

$$r = xcos(\theta) + ysin(\theta) \tag{2.2}$$

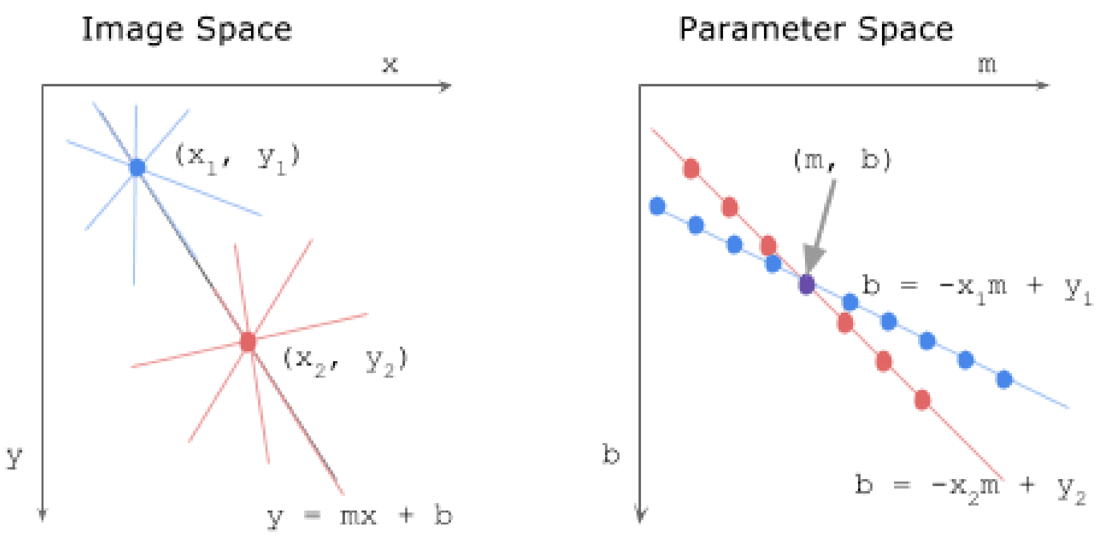

Figure 2.10: Hough transform detection method (Source: Quek, 2018)

Chapter 3

Results and Discussion

This chapter will discuss the results obtained from the methodology that has been explained in previous chapter. two major points that will be discussed in this chapter. First, the reliability of the methodology. As what has been explained in subsection 2.2.1, the two different approaches will be compared and discussed thoroughly. The second point is the result of the lip seal deformation where the result will be compared with FEM model and previous research.

3.1 Methodology Results

The methodology that has been done in this research requires two different approaches (See 2.2.1). However both of the approaches requires initial calibration, hence, the calibration result will be the starting point in this section. Thereafter, the two different approaches will be compared with each other.

3.1.1 Calibration

As can be seen on figure 3.1, the result is obtained by running *for loop* on the boundary locations, and identifies between two coordinates located on the same y-coordinate. As the *for loop* identifies two coordinates, the absolute value between the corresponding x-coordinates is taken. The result shows peak at the distance of 23 which means that the one millimeter distance is separated between 23 pixels. However, the plot also shows relatively high peaks between 18 until 24 pixels. This is caused by the edge detection approach. Looking back at figure 2.7, the boundaries detected also shows some squiggly lines resulting on this high peaks. Since these peaks have lower frequency than the number of frequency of 23 pixels, it can be considered as errors and can be neglected. Another point that need to be explained is the result on 0 pixel.

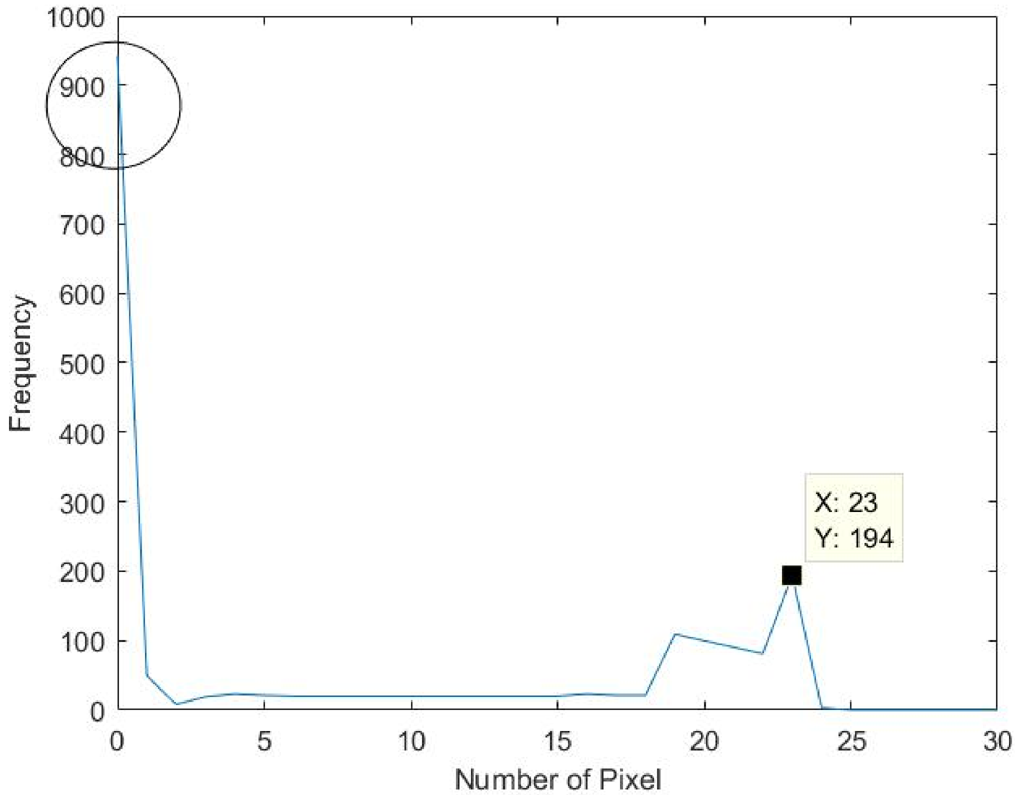

Figure 3.1: Absolute distance value between two x-coordinates (x-axis) of the boundaries and number of frequency (y-axis)

The frequency of 0 pixel is the highest due to the *for loop* that runs through all the boundaries locations that has the same y-coordinate. The result from 0 pixel is not important in this measurement, however, this result need to be clarified by virtue of clarity for the reader.

3.1.2 Contact Area Width Measurement

The purpose of this subsection is to give clarity on choosing the contact area width distance from the edge detection approach. As can be seen on figure 3.2 and figure 3.3, both of the measurements is taken from two different locations which results in two different results. figure 3.3 shows a clear single peak on the measurement whereas multiple peaks is found on figure 3.2. These high peaks shows that there are more than one measurements of contact area width in a single image. Despite the multiple peaks, the highest frequency in that image is taken which can represent the contact area width at that particular point.

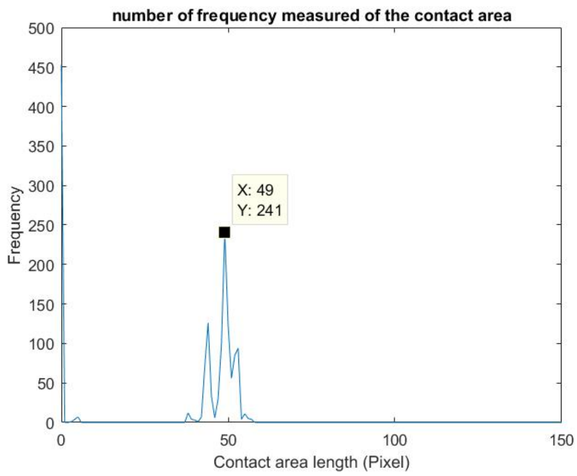

Figure 3.2: Measurement with various peaks

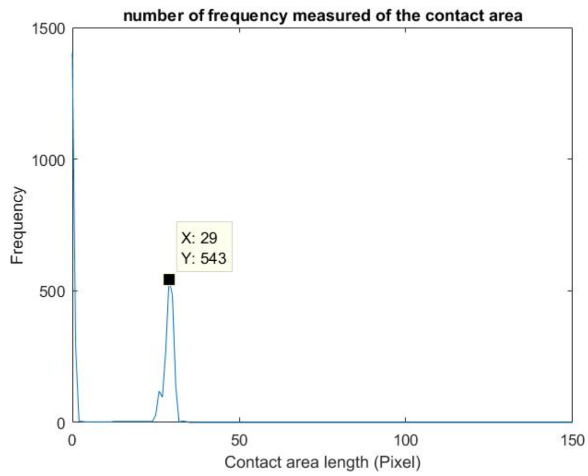

Figure 3.3: Measurement with 1 peak

3.1.3 Method validity

The results from edge detection approach is compared with the results from the Hough transform approach. As can be seen on figure 3.4, the contact area width is measured with 2 different approaches. The dotted lines were the result from the edge detection approach while the solid lines were the result from the Hough transform approach. Despite the small errors between two approaches, both approaches resulted in similar deformed contact area width profile. two remarks can be concluded from these results. First, the measurement of the contact area width from both of the measurement are very similar. Secondly, this measurement supports the validity of the measured contact area boundaries positions which will be explained on the following sections.

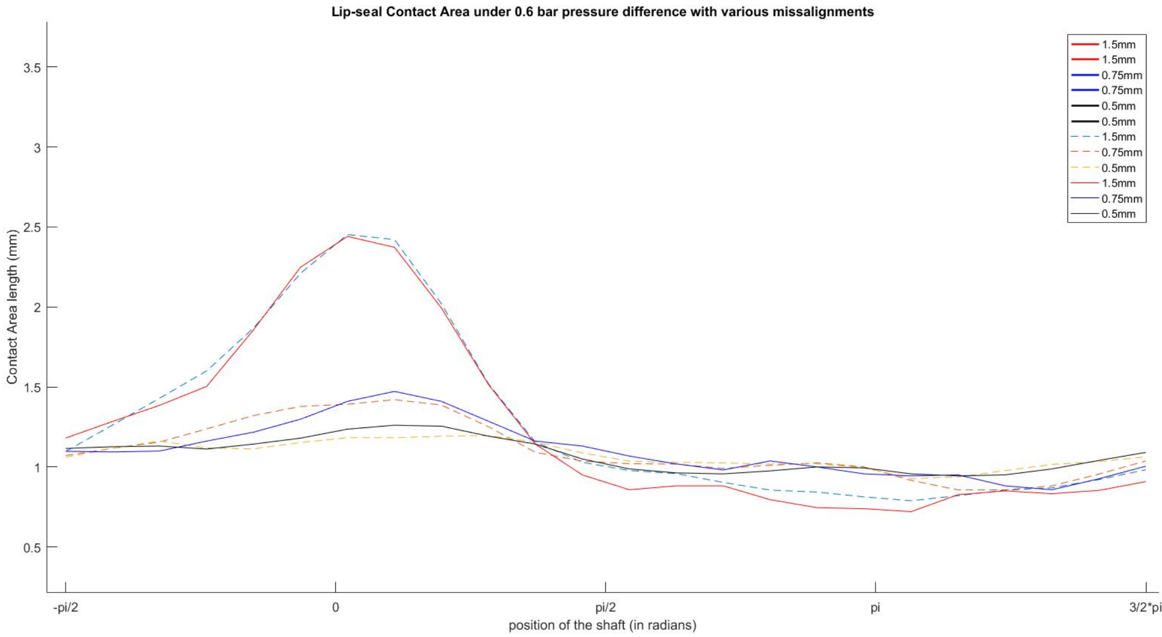

Figure 3.4: 0.6 Bar pressure difference with various misalignments

3.2 Lip Seal Deformation Results

This section will firstly describe the deformed lip seal profile under pressure difference and various misalignments. Subsequently, the FEM result of the deformed lip seal profile under pressure difference and various misalignment will be described. The comparison between the measurement and the FEM simulation will be discussed on the following section.

3.2.1 Deformation under Pressure Differences

The results shown on figures 3.5, 3.6, and 3.7 show the deformation of the lip seal under various pressure differences on static misalignments. The top side of the seal is referred to the oil side and conversely the air side for the bottom side. As the pressure difference increases, two main features can be identified. The first feature shows that regardless of the misalignments applied on the lip seal, the contact area width increases as the pressure difference increase. Second, the contact area width shifted downwards.

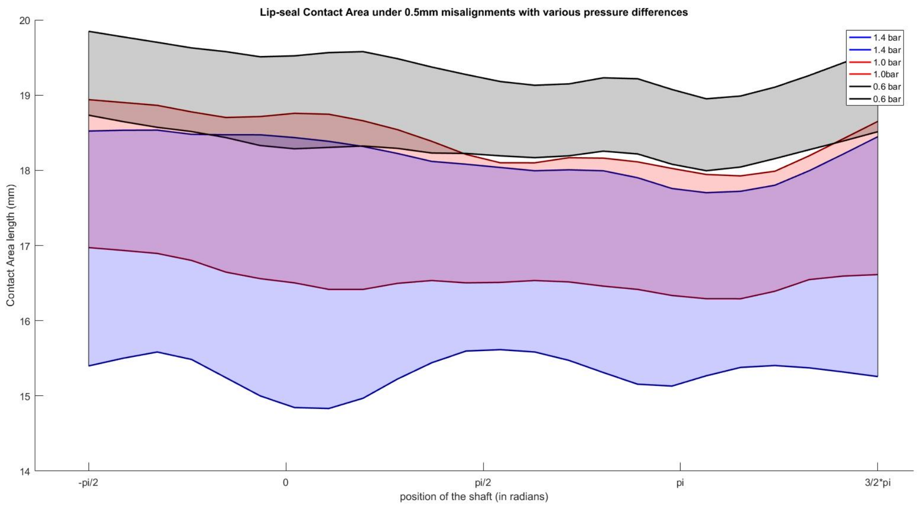

Figure 3.5: Deformed contact area under 0.5mm misalignment with various pressure difference

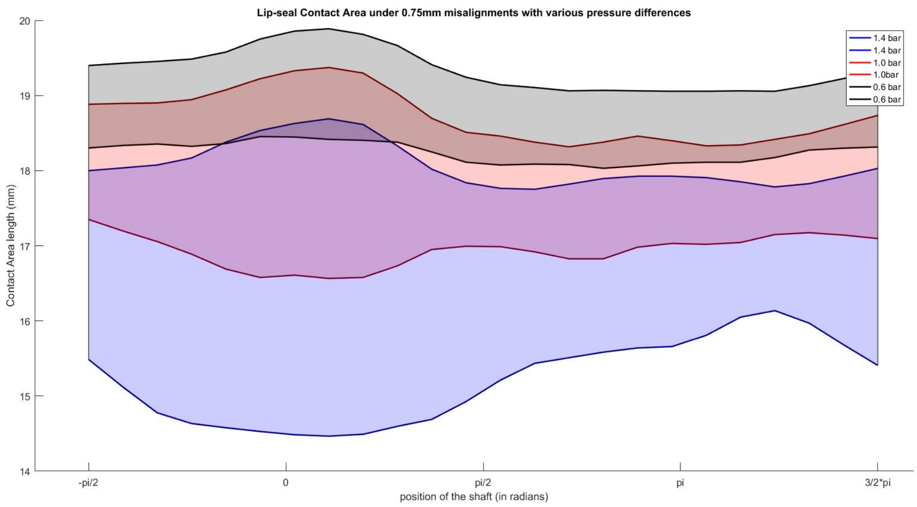

Figure 3.6: Deformed contact area under 0.75mm misalignment with various pressure difference

3.2.2 Deformation under Misalignments

On figure 3.8 The 1.5mm misaligned lip seal shows sinusoidal-alike contact area boundaries location deformation profile, where the other two measurements does not show similarities on the sinusoidal alike deformation profile. However, on the air side, the measurements from the 1.5mm and 0.5mm misalignments show a jutted bump on the oil side of the lip seal. On the opposite side of the misaligned point, the 0.5mm and 0.75mm misaligned lip seal profiles shows a small engraved curvature at the $\frac{\pi}{2}$ angular position of the shaft (it is easier to notice on figures 3.5 and 3.6).

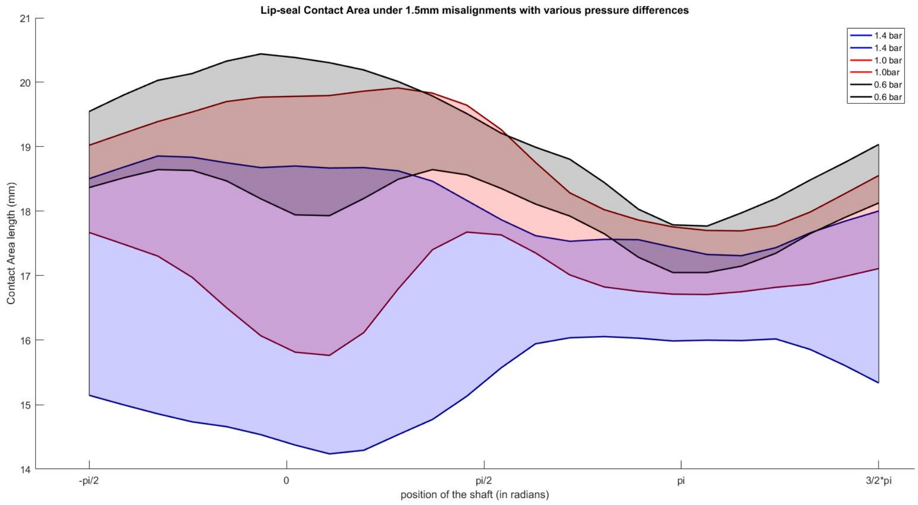

Figure 3.7: Deformed contact area under 1.5mm misalignment with various pressure difference

As the pressure difference is increased to 1.0 bar (see fig 3.9), the increasing contact area width at misaligned point are shown from all three measurements. In addition, the growth of the contact area width on the air side is longer than the oil side showing the jutted bump more conspicuous than the measurement under 0.6 bar pressure difference. At $\frac{\pi}{2}$ radial position of the shaft, the deformed lip seal profiles of 0.5mm and 1.5mm show the sinusoidal-alike deformation profile, on the other hand, the 0.75mm misaligned lip seal profile does not show the similarity with the other two measurements, however the sinusoidal-alike boundaries profile can be seen on the oil side.

The last measurement can be seen on figure 3.10 where the pressure difference is set at 1.4 bar pressure difference. The thickening of contact area width from all measurements misaligned lip seal at misaligned point shows the similar profile. However, the jutted bump on the air side is barely visible.

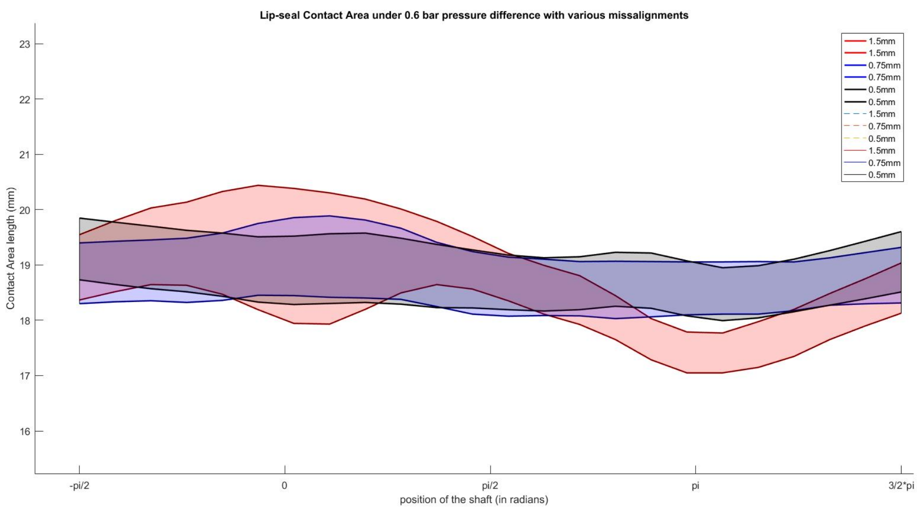

Figure 3.8: Deformed contact area under 0.6 bar pressure difference with various misalignments

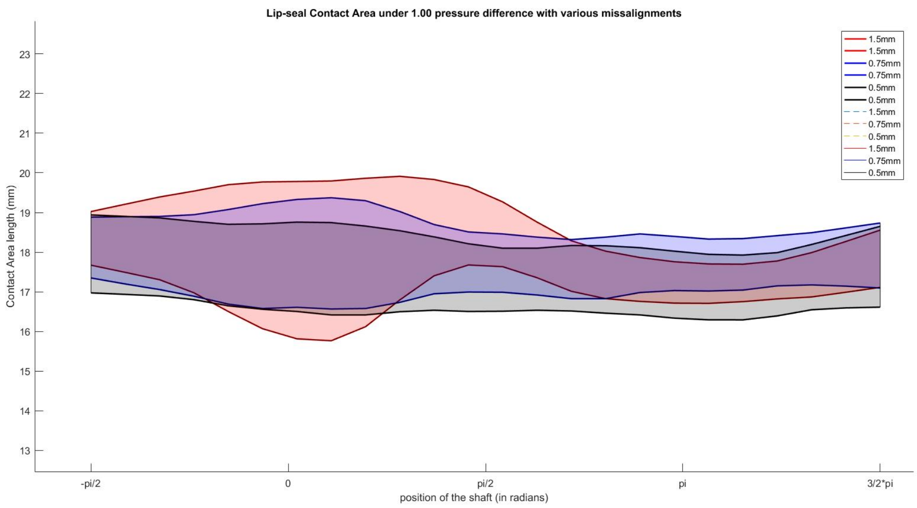

Figure 3.9: Deformed contact area under 1.0 bar pressure difference with various misalignments

3.2.3 FEM results on Deformation under Pressure Difference and Misalignments

In this subsection, the FEM simulation results, from pressure difference and various misalignments will be addressed. To begin with, The FEM result from the pressurized seal will be firstly described. As can be seen on figure 3.11, the FEM simulation only captured where the lip seal is under no static eccentricity. The air side surface of the lip seal extends towards the bottom housing on axial direction causing the

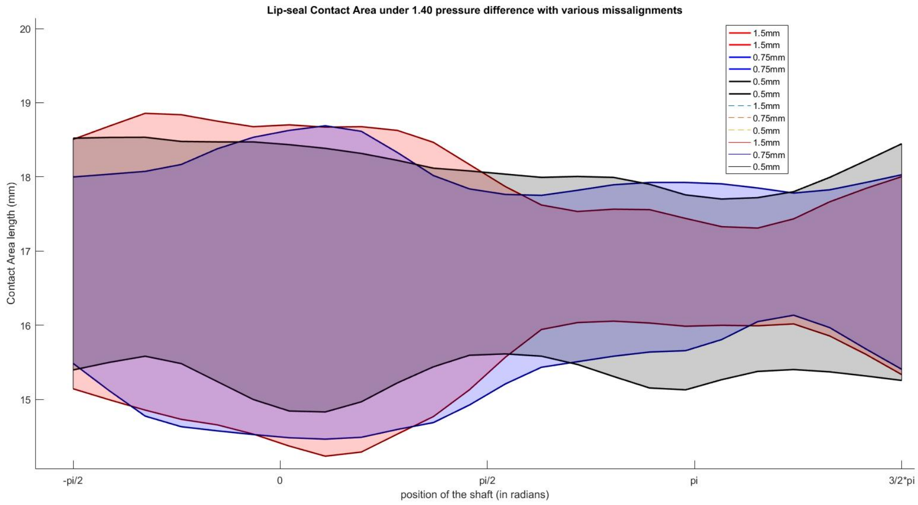

Figure 3.10: Deformed contact area under 1.4 bar pressure difference with various misalignments

contact area to grow. Another deformation is the oil side boundaries shifted towards the bottom housing. It is also necessary to be stated that the FEM simulation are performed using zero friction coefficient between the lip seal and the glass shaft and thus the contact width differ from the actual measurement which is measured on a non-zero friction coefficient.

The FEM simulation result of the deformed lip seal under zero pressure difference and under various misalignments are shown on figure 3.12 where the misalignment is applied at radial position zero. Again, the simulation is simulated with zero friction coefficient between the lip seal and the glass shaft. Three observations can be identified from the simulation model. First, the contact area width increases where the misalignment applied at. This occurrence also observed by Bavel [4], in addition, Bavel's observation also shows that the increase of the contact width on the air side is larger than the oil side. Second, the contact area boundaries around the misaligned point shifted upwards while the opposite of the misaligned point shifted downwards yielding a sinusoidal-shaped lip seal contact boundaries. Third, the contact area width from all measurements on figure 3.12 yield in a relatively equal width thickness at radial position of $\frac{\pi}{2}$ and $\frac{3\pi}{2}$ making the contact area profile axially symmetric at $\frac{\pi}{2}$.

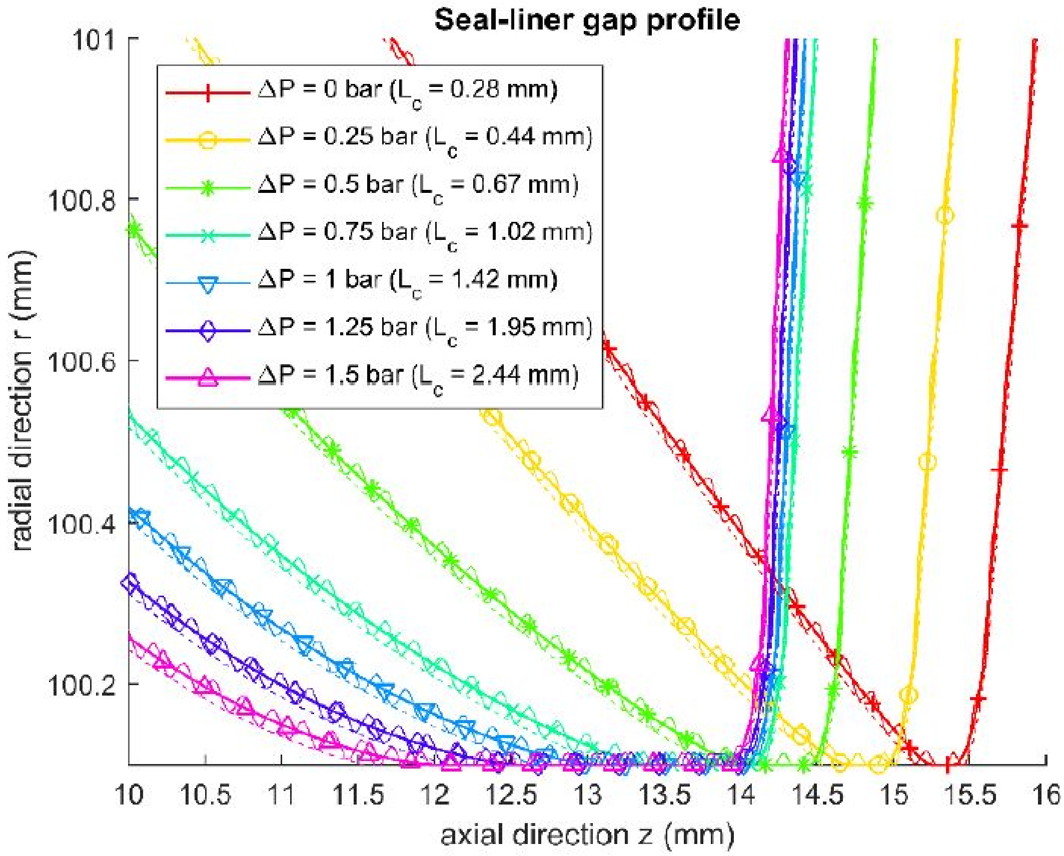

Figure 3.11: Seal liner gap profile under various pressure differences (Source: Borras, on going research)

3.3 Discussion

In this section the methodology results and the lip seal deformation results will be discussed. During the measurement, the researcher had encountered unexpected problems during the image acquisition. However, the results from the image analysis is still credible. Therefore it is necessary to explain what had happened during the execution of the methodology and how to encounter the problems where this explanation will be useful for future measurement purposes. The second part of this section will discussed the geometry of the deformed lip seal. The previous section explained about how it deformed. In this section the results from the actual measurement will be compared with the FEM simulation. Consequently, the reasoning of the deformation will be delivered, in addition, the reasoning of the lip seal deformation will be associated with the contact pressure and radial forces.

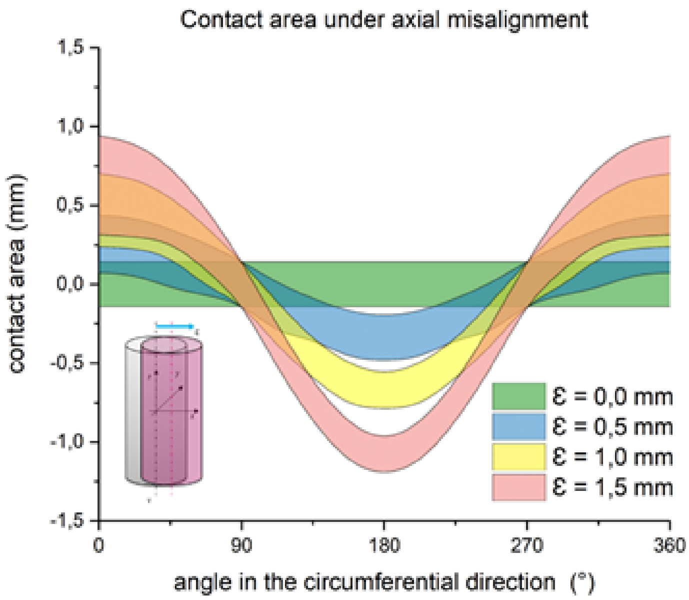

Figure 3.12: Lip seal deformation profile under 0 bar pressure difference various misalignment (Source: Borras, on going research)

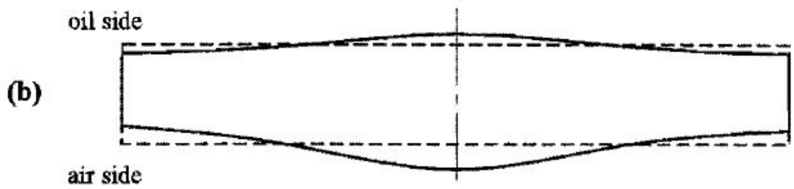

Figure 3.13: Bavel's observation when Lip Seal is applied with static eccentricity (Source: Bavel, 1997)

3.3.1 Methodology Discussion

During the execution of the methodology, the research encountered a problem during the image processing for the hough transform. As can be seen on figure 2.8 the image has bright color intensity compare to the background and therefore the detection of the boundaries by the program is relatively easy. On figure 3.14, the image acquired has an extreme low intensity level of red color thus the detected deformed boundaries is barely observed. To encounter this problem, red-colored filtration is used, resulting on relatively high intensity level which then converted into gray-scale image. Although the image is filtered with red color, the intensity level of the bottom housing is relatively high enough than the deformed lip seal, thus, the bottom housing is still captured in the gray-scale image.

The problem does not stop on the intensity level of the image. Before the image can be converted into binary image for boundary detection, the *threshold* function detected only the bottom housing. However, from the function itself, the threshold intensity level is acquired. The measurement process can be separated into two steps. First, the detection of the bottom housing boundaries position which represents the reference point and secondly, the detection of the lip seal boundaries. In order to achieve the first step, the threshold intensity level is inputted manually, where the inputted intensity level must be higher or equal to the intensity level that acquired from the *threshold* function. Consequently, the inputted intensity level must be lower than the intensity level that acquired from the *threshold* function in order to detect the lip seal boundaries position. However the inadequacy of manually inputting the threshold intensity level comes with 2 drawbacks. Setting the threshold too low will yields of distorted image where the boundaries detected is not the actual boundaries, on the other hand, setting the threshold too high generates a total darkness on the image. To assure that the detected boundaries is correct, the detected boundaries is then compared with the gray-scale image as what presented on image 2.10. The manually filtered two steps image processing can be seen on figures 3.15 and 3.16.

Figure 3.14: Extreme acquired image where the intensity of the image is low

Figure 3.15: Low-filtered threshold binary image

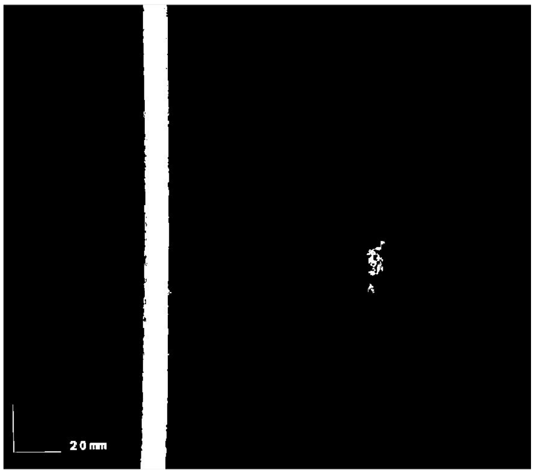

Figure 3.16: High-filtered threshold binary image

3.3.2 Lip Seal Deformation Discussion

As has been explained on this chapter introduction, the FEM calculations will be compared with the actual measurement. To start with, the result from the applied pressure difference will be discussed. As the pressure difference is increased, the FEM simulation shows (see figure 3.11) two distinctions that already stated in subsection 3.2.3. Both of the distinctions can also be seen on the actual measurement. The contact area boundaries shifted downwards due to the pressure difference that generates tangential force (see figures 3.5 , 3.6 and, 3.7) on the oil side towards the air side. As the pressure difference is increased more, the force acting on the oil side increases, causing the angle β to increase and the angle α to decrease (see figure 1.2) yielding the increase on the contact area width.

As the deformation of the pressure difference has been explained previously, now, the misalignment variable is added to the deformation of the lip seal. As already been stated on previous subsection, there are three major points that can be observed from the FEM simulation. However, all these three major points are only shown by several actual measurements. The sinusoidal shape profile of the contact area boundaries location can be seen directly on figures 3.8 and 3.9 under 1.5mm misalignment. However, the sinusoidal shape profile is not similar as the FEM simulation. From the actual measurement, it can be seen that the minimum contact area boundaries is not at $\frac{\pi}{2}$, instead, it is located close to the expected location. So does the maximum contact area width location, it shifted from the misaligned point where it is expected. The last major point is that the contact area width is not equal at $\frac{\pi}{2}$. From this non-similarities it can be concluded that the misaligned measurement result is not axially symmetric at $\frac{\pi}{2}$, therefore, in subsection 3.2.2, the deformation of the lip seal contact area boundaries location is defined as sinusoidal-alike. Despite the non-similarity of the contact area boundaries location profile, the deformation of the contact area width is indeed similar to Bavel's observation, where the increase of the contact area width around air side is bigger than the oil side. This observation can be seen on figure 3.8 under 1.5mm misalignment and figure 3.9 under all misalignment measurements.

Before discussing the sinusoidal contact area boundaries location profile, two types of forces that acts around the contact area must be first defined. Refering to Tasora's research [9], the radial load F_p has dimensions of a force but it has not a vectorial nature since it lacks a point of application. On the other hand, F_r is radial force, having radial direction and applied to the shaft. Per definition, the radial force is the force required to move the shaft radially from the perfectly centered position. The radial force is not null only when the shaft is eccentric.

To understand the sinusoidal-shaped contact area boundaries location profile, assume that no pressure difference is applied and the friction coefficient is largely higher than the friction coefficient that has been used in the FEM simulation. The deformed lip seal contact boundaries will only show enlargement in the contact area width where the misalignment is applied, and the rest of the contact area slightly reduced as shown in figure 3.13. Look back on figure 1.2, around the misaligned point, the bottom housing is pushed towards the glass shaft generating net positive radial force (positive radial force is defined as upward direction) against the tip of the lip seal [9]. Because the hinge point is fixed, this point acts as the rotation axis of the lip seal and combining with the force generated on the tip of the seal, it generates positive moment (positive moment is defined on counterclockwise direction) which makes the tip of the lip seal rotates upwards on the axial direction and followed by the increase of the angle β. In addition, the angle on the air side α decreases yielding in increase of the contact area width. This occurrence explain the deformation observed by Bavel, however, this is not enough to explain the sinusoidal contact area boundaries. To understand how the sinusoidal contact area boundaries location profile, assume that the friction coefficient between the shaft and the seal is reduced to a great extend. As the lip seal rotates counterclockwise, the tip of the seal slides along the axial direction towards the top housing bringing over the air side at the same time. This explain the elevation on the misaligned point. On the opposite side of the misaligned point, the glass shaft shifted away from the tip of the seal, the garter spring generates negative radial force on the tip of the seal (see figure 1.2) causing a negative moment of the lip seal, generating angle β to decrease and angle α to increase. And again, due to the low friction coefficient, the tip of the lip seal slide downwards.

The combination between both of misalignment and the pressure difference can be seen on the measurement results (see figures 3.8, 3.9 and, 3.10). From 0.6 bar and 1.0 bar pressure differences, the lip seal contact area boundaries shifted downwards, moreover, the sinusoidal-alike deformation profile is occurred as what has been stated in the first and second paragraphs. As the pressure difference increased to 1.4 bar, the curvature decreased on the air side of the lip seal boundaries causing no bump that jutted out. The pressure difference is now relatively high and the maximum contact area width is almost reached, hence, the gulf-formed boundaries started to disappear except on 0.5mm misalignment. The limitation of the maximum contact area width is shown when the contact area width of 0.75mm misalignment approaches the size of the contact area width of 1.5mm misalignment (see figures 3.9 and 3.10). Simultaneously, the sinusoidal-shaped deformation profile of the lip seal slowly vanishes. This is due to the maximum stretching of the contact area width on the air side and the high pressure difference that pushes down the lip seal contact boundaries location resulting back to Bavel's observation.

Predicting Contact Pressure and contact load

An essential parameter on lip seal application is contact pressure and radial load. To prevent confusion between radial force and radial load, from this section until the end of this report, the radial load is addressed as contact load. It is important to understand these parameters because it is commonly used in practical engineering to predict leakage, durability, expected life, maximum allowed speed and etc. Before discussing deeper about these topics, contact pressure and contact load must be defined beforehand. The total contact load is the combined action of the garter spring and of the lip seal deformation [9], in addition to that, the total contact load can be calculated by integrating the contact pressure along the contact area, hence, It is now clear the definition and relation between the contact pressure and contact load. This can be reformulated as mathematical equation which is expressed in equation 3.1

$$F_p = \int p(\theta, z(\theta))dA \tag{3.1}$$

As has been stated above, the contact area width increases at misaligned point and when the pressure difference increases. As the contact area width increases under pressure difference, the contact pressure peak increases until a certain point and it starts to decrease, moreover, the contact pressure along the contact area shows a relatively small increase compare to the peak yielding a bell mouth-shaped pressure distribution along the contact area width [10] (see figure 3.17). From this measurement, it can be reasoned, under all predefined conditions, that the contact load between the lip seal and the shaft is a function of pressure difference of the fluid that act around the lip seal, the contact area (or fitting) between the lip seal and

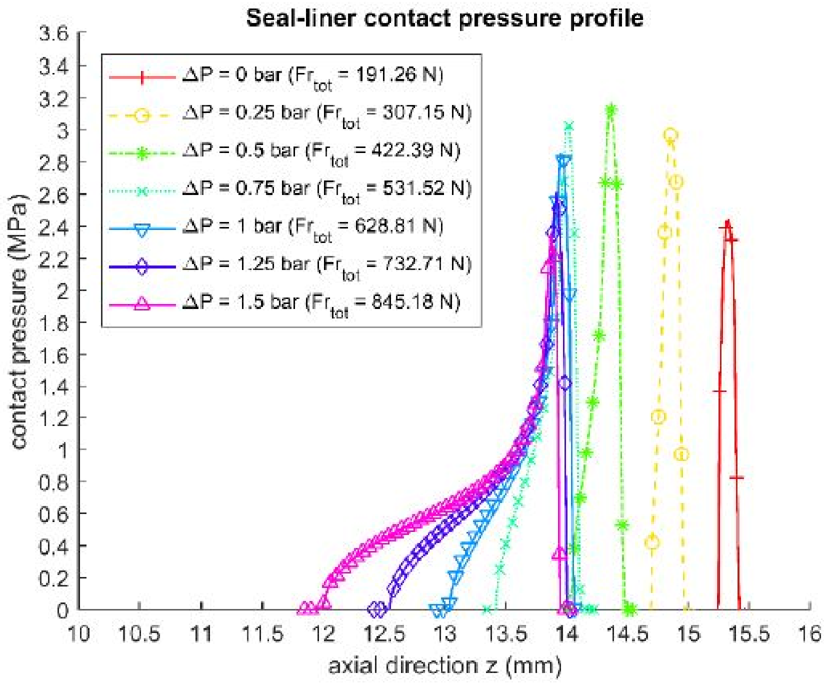

Figure 3.17: Contact pressure distribution under various pressure difference with zero friction coefficient (Source: Borras, On going research)

the shaft, and the material properties of the lip seal. This can be mathematically formulated as been stated by equation 3.2. Since this measurement uses the same material properties, the influence of the material properties can be neglected.

$$F_p = f[\psi, \Delta p, \text{material}] \tag{3.2}$$

$$P = \frac{F}{A} \tag{3.3}$$

However, this measurement does not give understanding on how the contact pressure nor the contact load change along the radial direction around the shaft. Based on Tasora's FEM measurement [9](see figure 3.18), the contact load is only marginally affected by the static eccentricity, whereas it depends more heavily on static interference and temperature. The measurement assumed that the friction coefficient between the lip seal and the shaft is 0.15. Therefore it can be assumed that the contact load to be constant along the radial direction around the shaft assuming that the pressure difference on the lip seal is kept constant.

From these two measurements that is stated above, assuming that both of the measurement performs similar profile for any friction coefficient between the shaft and the lip seal, the contact pressure distribution along the radial direction and along the axial direction for can be predicted. By using Pascal's formula (see equation 3.3),

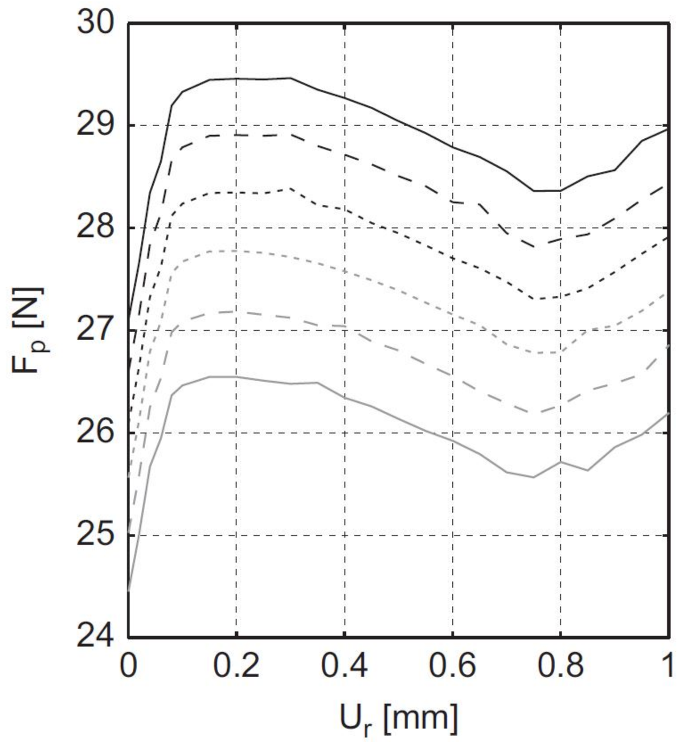

Figure 3.18: Contact load curves for a given set of material parameters, for initial interference of 0.75mm (Source: Tasora,2012)

the contact pressure on the radial direction would be the lowest on the point where the misalignment is applied. Subsequently, by implementing the contact pressure profile measurement along the axial direction [10], the lowest peak would be captured on the misaligned point where the contact area width increases the most. On the contrary, the highest peak would be shown on the opposite side of the misaligned point.

Chapter 4

Conclusions

To summarize, a method to measure a deformed pressurized lip seal has been made. The method uses two different approaches where both approaches resulted on an alike profile of contact area width, hence, it validates the measurement of the lip seal boundaries profile deformation. The observed deformed lip seal boundaries profile shows several similarities profiles as the FEM models and preceding research, thus, the contact area boundaries profile deformed as the expected deformation. In conclusion, this research has answered the two main problems stated on section 1.3.

4.1 Future Research

For future research, determination of the contact pressure would be essential. As what has been stated on subsection 3.3.2, the contact pressure will be dependent on the contact area and the contact load, the contact area itself is dependent on three variables which are; radial position, pressure difference, and the static eccentricity. Therefore, a 3D FEM simulation is proposed to understand contact pressure distribution profile. Therefrom, the contact load can be studied further to understand whether the assumption of constant contact load around the shaft is acceptable. Both of the parameters are really important for practical engineering purposes to determine leakage, wear, and other occurrences.

4.2 Acknowledgement

To M.B. de Rooij to give an opportunity for me to be able to contribute on this project, To F.X. Borras for giving insight and discussions, To E. de Vries and R.Meijer for the expertise on measurement and equipment. I would like to acknowledge my parents who have supporting me mentally and financially during the whole of my study.

Bibliography

[1] M. Mokhtar, M. Mohamed, M. El-Giddawy, and S. Yassen, “On the effect of misalignment on the performance of u-type lip seal,” *Wear*, vol. 223, no. 1-2, p. 139142, 1998.

[2] X.-G. SONG, L. WANG, and Y.-C. PARK, “Analysis and optimization of nitrile butadiene rubber sealing mechanism of ball valve,” *Transactions of Nonferrous Metals Society of China*, vol. 19, pp. s220 – s224, 2009.

[3] B. Wennehorst, *On Lubrication and Friction in Soft Rough Conformal Sliding Contacts*. PhD thesis, universitt Hannover, Dec 2016.

[4] P. Bavel, van, *The leakage-free operation of radial lip seals*. PhD thesis, Technische Universiteit Eindhoven, 1997.

[5] J. F. Postmes, “Influence of pressures and misalignment on leakage and tipping point of stern tube seals,” *Academic Research Skills, Twente University*, Jan 2019.

[6] J. Karsten and Q. M. Palmers, “Determination of the contact area of a rubber lip seal against a shaft with different pressures and misalignments using total internal reflection,” *Academic Research Skills, Twente University*, pp. 119 – 126, Dec 2018.

[7] C. Hidrovo and D. Palmers, “Development of a dual purpose visualization technique for the study of rotating shaft seals,” *Proceedings of the 3rd AMS/JSME Joint Fluids Engineering Confference*, 1999.

[8] M. Stakenborg, “On the sealing mechanism of radial lip seals,” *Tribology International*, vol. 21, no. 6, p. 335340, 1988.

[9] A. Tasora, E. Prati, and T. Marin, “A method for the characterization of static elastomeric lip seal deformation,” *Tribology International*, vol. 60, pp. 119 – 126, 2013.

[10] F. Borras, M. Bazrafsah, M. de Rooij, and D. Schippers, "Pressurized lip seals: multi-scale modelling approach to contact," on going research.

Appendix A

Boundary detection codes

In this chapter, the codes to measure the contact area width will be given, several section is skipped due to repetition, however the essential part will not be skipped. The codes for the calibration is similar to the edge detection approach from which are shown on figure A.1 until figure A.5. The Hough transform codes are shown from figure A.6 until figure A.8

A.1 Boundary Detection Codes

Figure A.1: part I

```
clear all;
close all;
clc;
img = rgb2gray(imread('calibrator2.jpg'));
imtool(img)

%inputing the image that shows the measurement

background = imopen(img,strel('disk',13));

figure
surf(double(background(1:8:end,1:8:end))),zlim([0 100]);
set(gca,'ydir','reverse');

I2 = img-background;
%imshow(I2);

I3 = imadjust(I2);
%imtool(I3);

level = graythresh(I3);
bw = im2bw(I3,level);
bw = bwareaopen(bw,50);
imshow(bw);

%imadjust is to increase the contrast of the image and converts the image
%into binary image. bwareaopen helps removing background noise
%
%-----------------------------------------------------------------------------------
```

```
BW = edge(bw,'canny');
%imshow(BW)

[B,L] = bwboundaries (BW,'noholes')
imshow(label2rgb(L,@jet,[.5 .5 .5]))



hold on
%figure(2)
%imshow(BW)
hold off

hold on
for k = 2:(length(B)-1);
    boundary = B{k};
[M(k),N(k)] =size(B{k,1});
  W = find(M>100);
 %(boundary (:,2), boundary(:,1),'w','LineWidth',2);
end
B_new = B(W);




for i = 1:length(B_new);
    boundary_new = B_new{i};
    plot (boundary_new (:,2), boundary_new(:,1),'k','LineWidth',2)
end
```

Figure A.2: part II

```
hold off

%
a = B_new{5,1}
b = B_new{6,1}
c = B_new{7,1}
d = B_new{8,1}
e = B_new{9,1}
f = B_new{10,1}
g = B_new{11,1}
h = B_new{12,1}
j = B_new{13,1}
l = B_new{14,1}


n =0




%

for i= 1:length(a);
    for k=1:length(a);
    if a(k,1) == a(i,1);
         aa(i)=abs(a(k,2)-a(i,2));

    end
    end
```

Figure A.3: part III

A.2 Hough Transform

```
end

binc_aa = [0:30];
counts_aa = hist(aa,binc_aa);
result_aa = [binc_aa; counts_aa]

binc_bb = [0:30];
counts_bb = hist(bb,binc_bb);
result_bb = [binc_bb; counts_bb]



binc_cc = [0:30];
counts_cc = hist(cc,binc_cc);
result_cc = [binc_cc; counts_cc]


binc_dd = [0:30];
counts_dd = hist(cc,binc_dd);
result_dd = [binc_dd; counts_dd]

binc_ee = [0:30];
counts_ee = hist(ee,binc_ee);
result_ee = [binc_ee; counts_ee]


binc_ff = [0:30];
counts_ff = hist(ff,binc_ff);
result_ff = [binc_ff; counts_ff]
```

Figure A.4: part IV

```


result_test = result_aa+result_bb+result_cc+result_dd+result_ee+result_ff+result_gg;
qqq = linspace (0,30,31)
ttt =result_test(2,:)

hold on
figure(5)
plot(qqq,ttt)
hold off

hold on
figure(7)
subplot(2,2,1),(imshow(img))
subplot(2,2,3),(imshow(I2))
subplot(2,2,4),(imshow(bw))
subplot(2,2,2),(imshow(background))

hold off
```

Figure A.5: part V

```
ar all;
se all;
;
is script is to analyze the distance between the housing and the
tected edge. The housing will hold as 'ground'.

 rgb2gray(imread('018.jpg'));
 = I(:, :, 1);
ad image
------------------------------------------------------------------------------

eate binary image

kground = imopen(I,strel('disk',100));

king the background spreaded evenly
ure
f(double(background(1:8:end,1:8:end))),zlim([0 100]);
(gca,'ydir','reverse');


= img-background;


= imadjust(I2);



el = graythresh(I3);
```

Figure A.6: part I

```
bw = bwareaopen(bw,70);


BW = edge(bw,'canny');


%%
[H,T,R] = hough(BW);
imshow(H,[],'XData',T,'YData',R,'InitialMagnification','fit');
xlabel('\theta'), ylabel('\rho');
axis on, axis normal, hold on;

P  = houghpeaks(H,5,'threshold',ceil(0.3*max(H(:))));
x = T(P(:,2)); y = R(P(:,1));
%plot(x,y,'s','color','white');

lines = houghlines(BW,T,R,P,'FillGap',5,'MinLength',7);
figure, imshow(I3), hold on
max_len = 0;
for k = 1:length(lines)
   xy = [lines(k).point1; lines(k).point2];
   plot(xy(:,1),xy(:,2),'LineWidth',2,'Color','green');

   % Plot beginnings and ends of lines
   plot(xy(1,1),xy(1,2),'x','LineWidth',2,'Color','yellow');
   plot(xy(2,1),xy(2,2),'x','LineWidth',2,'Color','red');

   % Determine the endpoints of the longest line segment
   len = norm(lines(k).point1 - lines(k).point2);
   if ( len > max_len)
```

Figure A.7: part II

```matlab

lines = houghlines(BW,T,R,P,'FillGap',5,'MinLength',7);
figure, imshow(I3), hold on
max_len = 0;
for k = 1:length(lines)
   xy = [lines(k).point1; lines(k).point2];
   plot(xy(:,1),xy(:,2),'LineWidth',2,'Color','green');

   % Plot beginnings and ends of lines
   plot(xy(1,1),xy(1,2),'x','LineWidth',2,'Color','yellow');
   plot(xy(2,1),xy(2,2),'x','LineWidth',2,'Color','red');

   % Determine the endpoints of the longest line segment
   len = norm(lines(k).point1 - lines(k).point2);
   if ( len > max_len)
      max_len = len;
      xy_long = xy;
   end
end

figure(3)
hold on
imshow(bw)
hold off


```

Figure A.8: part III